



Harmonic Content of A_p Index

Marek Vandas¹, Evgeny Romashets², Tasmina Imam², Tanvir Hasan², Pranab Majumder², and Sanjay Karki²

¹Astronomical Institute of the Czech Academy of Sciences, Prague, Czech Republic

Correspondence: Evgeny Romashets (eromashets@lamar.edu)

Abstract. Zajtsev et al. (1993) applied fast Fourier transform (FFT) (Cooley et al., 1969) of the magnetic field components measured by a particular magnetic observatory. They reported that some patterns could be recognized in the contour plots of Fourier coefficients versus time for different phases of sub-storm evolution. Similar techniques can be applied to the planetary geomagnetic indices A_p and D_{st} . The spectral content changes prior to the growth phase of the sub-storm. The higher frequency coefficients, the larger the power spectrum is shifted upwards. This feature can serve as a precursor, if spotted. We present an analysis of the February 2001, 2003, and 2017 time intervals. The technique can be potentially used as a forecast tool for predicting geomagnetic activity.

1 Introduction

Abe et al. (2023) analyzed Disturbed storm time index (D_{st}) and Sunspot Number (SSN) data using FFT. Their study explored geomagnetic storm occurrences during the solar cycles 23 and 24. The study of De Michelis et al. (2014) explores the connection between spatial and temporal Fourier spectra in the geomagnetic field, making assumptions about the spatial power spectrum and its time derivative. It reveals that, under these assumptions, the temporal spectrum at the core-mantle boundary follows a power-law behavior with a negative spectral exponent, findings corroborated by magnetic observatory data. Additionally, the paper suggests practical approximations for the temporal spectrum at the Earth's surface, emphasizing the relevance of its outcomes within a potentially chaotic dynamics governing the generation and maintenance of the geomagnetic field.

Rangarajan and Lyemori (1997) analyzes K_p and A_p indices from 1932 to 1960, using modern techniques to examine their time variations. Even if 35 years (1961–1995) of data were added, the relative frequencies of K_p with different magnitudes show consistent seasonal and solar-cycle dependencies.

De Gonzalez et al. (1993) investigated 51 years of monthly and daily samples of the A_p geomagnetic index (1932–1982) using the power spectrum technique. The monthly A_p power spectrum reveals a period around 4 years, associated with a double peak structure in geomagnetic activity. Daily A_p spectrum peaks are interpreted as harmonics of a 6-month period, and others as linked to solar rotation periodicity, suggesting the juxtaposition of two Fourier sequences.

In their analysis of the D_{st} index using singular spectrum analysis, Le Mouel et al. (2019) identified several significant components. The D_{st} series exhibited a dominant trend, followed by a prominent 6-month component. Additionally, they

²Department of Physics, Lamar University Beaumont, Texas, USA





found a 47-year component, along with the well-known 10.6-year solar cycle. Furthermore, they detected a secondary seasonal line at 1 year. Notably, common pseudo-harmonic components at 22, 11, and 5.5 years were observed across all indices, indicating solar activity influences. The study highlighted the complex nature of these components, showcasing variations in frequency and amplitude, and emphasizing the intricate mechanisms governing solar-terrestrial relationships through detailed phase relationship analyses.

Rigozo et al. (2006) applied multiple-taper spectral analysis to the annual and monthly average series of aa, A_p , and R_z from 1868 to 2001. Using a single taper in spectral analysis reduces bias from spectral leakage but also decreases sample size and information retention.

Riabova and Spivak (2018) did this kind of analysis of the K_p index as a characteristic of the geomagnetic activity at the Mikhnevo Geophysical Observatory from 2009 to 2015 using the adaptive smoothing method.

Riabova (2018) developed a wavelet model for analyzing geomagnetic field variations, aiming to address the complex structure of geomagnetic data and detect anomalies efficiently. By utilizing raw second data from observatories and post-processed minute data, the model's numerical implementation enabled online analysis and demonstrated effectiveness in detecting sudden geomagnetic anomalies, especially preceding and during magnetic storms, while considering noise effects.

Shnirman et al. (2009) investigated the longitudinal asymmetry in solar activity evolution by applying the wave packet technique to the period domain of 25–31 days, centered at the 27-day solar rotation period, for both sunspot number and geomagnetic *aa* index data. The researchers observed alternating smaller and larger amplitudes of the 11-year solar cycle, resulting in a 22-year periodicity in the 27-day signal.

Idosa et al. (2023) did wavelet-approach based study to investigate the relationship between cosmic ray activity and various solar and geomagnetic indices, including the solar flare index, coronal index, K_p , auroral electrojets, A_p , D_{st} , polar cap, L_{α} , H_p60 , and A_p60 indices. Using wavelet-based approaches, they analyzed data from ground-based neutron monitor stations at the KIEL and MOSC stations during the years 2003 and 2004. In addition, data from different sources were incorporated to obtain information on the different indices examined in the study.

The study of Ahluwalia (2000) explores the relationships between the planetary index A_p , the magnitude of the interplanetary magnetic field (B), and the bulk speed of the solar wind (V) from 1963 to 1998, revealing a long-term trend in B corresponding to A_p variations, with B being more fundamental than V in influencing A_p .

Campbell (1973) studied the geomagnetic field data in 1965 and found that field amplitudes increase linearly with periods, with nearly equal northward and eastward components at all latitudes and stronger values in auroral and equatorial regions, showing seasonal variations and highest field values at 65° to 75° geomagnetic latitude, with most magnetic energy concentrated between 60° and 80° latitude.

The study of Pai and Sarabhai (1964) examines periodic fluctuations in the Earth's magnetic field during magnetic storms using data from 1958. Autocorrelation analysis reveals a common 40-minute period for fluctuations, primarily during storm phases. Fluctuations are synchronous at equatorial stations but irregular and uncorrelated at higher latitudes. The scale length of inhomogeneities in solar plasma causing fluctuations is estimated at 0.02 a.u., comparable to other studies.





Cliver et al. (1996) proposed that the 22-year cycle in geomagnetic activity, associated with alternating sunspot maxima within Hale cycles, is primarily driven by solar variations, including stronger 27-day recurrent wind streams during declines of even-numbered solar cycles, which contribute to increased geomagnetic activities.

Love (2011) analyzed K_p -index data from geomagnetic observatories in Germany, Britain, and Australia from 1868 to 2009, covering the solar cycles 11 to 23. It finds that geomagnetic activity has generally increased over this period, with German data showing consistently higher disturbance levels compared to British and Australian data. The occurrence of magnetic storms during the declining phase of sunspot-solar cycles is evident in the solar cycles 14 to 23 but less so in the cycles 11 to 13, suggesting a change in solar-terrestrial interaction over the past 141 years.

Delouis and Mayaud (1975) analyzed 103 years of 3-hour aa indices and K_p indices from two antipodal observatories, finding stable lines for semiannual and annual variations, and less stable lines for the 11-year and 90-year cycles. No significant line corresponded to the 27-day sun rotation, but clusters of unstable lines were associated with increased background noise, suggesting an average speed of 27.1 days for recurrent emitting sources (sunspots + M regions). No Moon influence was detected, and all lines (significant or not) were in phase between hemispheres. The study proposed a distinction between the astronomical (modulation) and astrophysical (excitation) lines.

The study of Zajtsev et al. (1993) analyzed digital magnetic-variation data from polar, auroral, and mid-latitude stations to investigate the energy spectra of very large storms and their uniform structure across latitudes, suggesting a link to Kelvin-Helmholtz instability waves in the low-latitude boundary layer of the magnetosphere.

2 Model

We consider the A_p index as a function of time that can be decomposed into the Fourier sum with the fundamental angular frequency $\omega = \frac{2\pi}{T}$, where the period is T=27 days. The index is calculated per three hour time interval, that is, the data in $K=27\cdot 8=216$ intervals are used. Consider the function $A_p(t)$ in the time interval $\left(\frac{l}{K}T,\frac{l}{K}T+T\right)$ where $l\geq 0$ is an integer, and introduce a function $A_{pl}(t')$ defined for $t'\in\left(-\frac{T}{2},\frac{T}{2}\right)$ by

$$A_{pl}(t') = A_p \left[t' + \left(\frac{l}{K} + \frac{1}{2} \right) T \right]. \tag{1}$$

The function $A_{pl}(t')$ is then (approximately) expressed as a finite Fourier series:

$$A_{pl}(t') = a_{0l} + \sum_{n=1}^{N} (a_{nl}\cos n\omega t' + b_{nl}\sin n\omega t') = c_{0l}\cos \phi_0 + \sum_{n=1}^{N} c_{nl}\cos n(-\phi_{nl}/n + \omega t').$$
(2)





Introducing discrete values $t'_{lk} = t_k - \left(\frac{l}{K} + \frac{1}{2}\right)T$, $A_p(t_k) = A_{p,k}$, $t_k = \frac{k}{K}T$, the coefficients a_{nl} , b_{nl} , c_{nl} , and phases ϕ_{nl} are calculated as follows:

$$a_{0l} = \frac{1}{K} \sum_{k=l}^{l+K} A_{p,k} - \frac{1}{2K} \left(A_{p,l} + A_{p,l+K} \right), \tag{3}$$

$$a_{nl} = \sum_{k=l}^{l+K-1} \left[\frac{K}{2n^2\pi^2} (A_{p,k+1} - A_{p,k}) (\cos n\omega t'_{l,k+1} - \cos n\omega t'_{l,k}) \right]$$

$$+\frac{1}{n\pi}(A_{p,k+1}\sin n\omega t'_{l,k+1} - A_{p,k}\sin n\omega t'_{l,k})\right], \ n > 0,$$
(4)

90
$$b_{nl} = \sum_{k=l}^{l+K-1} \left[\frac{K}{2n^2\pi^2} (A_{p,k+1} - A_{p,k}) (\sin n\omega t'_{l,k+1} - \sin n\omega t'_{l,k}) \right]$$

$$-\frac{1}{n\pi} (A_{p,k+1} \cos n\omega t'_{l,k+1} - A_{p,k} \cos n\omega t'_{l,k}) , \quad n > 0,$$
 (5)

$$c_{0l} = |a_{0l}|, (6)$$

$$c_{nl} = \sqrt{a_{nl}^2 + b_{nl}^2}, \ n > 0 \tag{7}$$

$$\phi_{0l} = 0, a_{0l} > 0 \tag{8}$$

$$95 \quad \phi_{0l} = \pi, \, a_{0l} < 0 \tag{9}$$

$$\phi_{nl} = \arctan(a_{nl}, b_{nl}), \ n > 0, \tag{10}$$

where \arctan of two arguments returns values in the full range $(0, 2\pi)$ and reduces to ordinary $\arctan \frac{b_{nl}}{a_{nl}}$ for $a_{nl} > 0$, $b_{nl} > 0$. Here, c_{nl} are amplitudes of the particular harmonics, and ϕ_{nl} are their phases, while a_{nl} and b_{nl} are Fourier coefficients. The coefficient a_{0l} is calculated via integration

100
$$a_{0l} = \frac{1}{T} \int_{-T/2}^{T/2} A_{pl}(t') dt'$$
 (11)

Because the function A_{pl} defined earlier is known only at times separated by three hours, we use linear interpolation, and the integration (11) becomes the sum of 216 areas of the corresponding trapezoids in (3). The summation is over k from k = l which corresponds to t' = -T/2, to k = l + K which corresponds to t' = T/2. The area between two points A_{pk} and $A_{p,k+1}$ is $(A_{pk} + A_{p,k+1})T/(2K)$. All A_{pk} appear twice, except the very first and the last in the sum, which appear only once.

Similarly, the coefficients a_{nl} and b_{nl} in (4) and (5) are calculated by integrations

$$a_{nl} = \frac{2}{T} \int_{-T/2}^{T/2} A_{pl}(t') \cos n\omega t' \,dt', \tag{12}$$

$$b_{nl} = \frac{2}{T} \int_{-T/2}^{T/2} A_{pl}(t') \sin n\omega t' \, dt', \tag{13}$$





which are replaced by sums with respect to k. The difference is that now each element of the sums is not simply the area of the trapezoid but the actual integral of the interpolated $A_{pl}(t')$ multiplied by $\cos n\omega t'$ or $\sin n\omega t'$ in the time interval of three hours.

Both c_{nl} and ϕ_{nl} depend on two indexes, in frequency and in time. The step along l corresponds to three hours in time, while a step along n means an increase in frequency by ω . In other words, all coefficients and phases are calculated in (3)–(5) for every three-hour interval. We used A_p data for the previous 27 days. N was set equal to K/2 = 108. The number of three-hour intervals in which the original function is defined equals the number of harmonics, sin and cos, in the Fourier sum. For any particular time, t, which is determined by k = t/3, time in hours, k in three-hour intervals from the beginning of the year, the allowed values of l are in the range (k-215,k-1), and the allowed beginning time of t is in the range (3k-645,3k-3). On the other hand, for a given l, there is only one set of coefficients a_{nl} and b_{nl} . It is shown in Figure 1 that the Fourier reconstruction of A_p is in good agreement with the original data. Fourier sum usually reconstructs functions better than the Fourier transform. Two-dimensional functions c_{nl} and ϕ_{nl}/n can be represented as contour plots. The idea is that abrupt changes in the A_p index can be predicted based on analysis of variations in Fourier coefficients before abrupt changes occur. In quiet periods, the low frequency coefficients dominate, but the magnitudes of higher frequency coefficients slowly increase just some time before the geomagnetic storm. The limit in a number of harmonics used for the reconstruction, N=108, can be explained in this way. There are 216 points in the interval. This means that the A_p index can change the sign of the derivative maximum 216 times. In the original data, the harmonics with frequency higher than this one are not present. One may think of a spline interpolation between the data points, which makes the function continuous and smooth. But interpolation brings assumptions about the values that are unknown. In addition to that, negative values may appear. What is more important, the interpolation will not bring higher frequencies. In the next section, we will show the calculated coefficients and phases for Februaries 2001, 2003, and 2017. The intervals contain relatively long quiet periods, with $A_p < 20$ nT, and strong disturbances with A_p up to 60 nT.

130 3 Results

The Fourier harmonics with N=108 work very well for February 2001, as one can see from Figure 1a. The original data and the reconstructed A_p are practically indistinguishable for most of the month. The reconstruction is done in the following way. For a given time t, the closest t_k is found that $t \le t_k$. The interval $\left(\frac{l}{K}T, \frac{l}{K}T+T\right)$, for which the coefficients a_{nl} and b_{nl} are calculated, is centered at t_k . This specifies the value of l: $l = \frac{K}{2T}(t_{k-1} + t_k - T) + 1$. Then a_{nl} and b_{nl} are determined from Eqs. (3)–(5) and the reconstructed $A_p(t)$ from Eqs. (1)–(2).

The month of February 2001 was relatively quiet, with $A_{p,\text{max}} = 40$ nT, without abrupt peaks. On the other hand, February 2003 was a very disturbed month, with $A_{p,\text{max}} = 70$ nT, and rapid transitions from a nearly smooth behavior changed to abrupt jumps. The reconstruction follows the data very well, but some minor deviations can be seen from time to time. February 2017 was a relatively quiet month. The reconstructed and real data are very close to each other.

140 Contour plots of c_{nl} are shown in Figure 2. In the contour plots, the horizontal axis represents time and the vertical axis represents n. The l is associated with time as it has been described above. It can be seen that maximum intensities are at low



150

155

165

170



frequencies. As frequency increases, the value of c_{nl} decreases. It is specifically interesting to observe zebra-type vertical bars, fibrils, on February 17–19, extending from n = 20 to 70.

Root mean square (RMS) values of the Fourier coefficients c_{nl} within harmonic bands (ranges of n) for every selected l (converted to time) are shown in Figure 3. So, it is a compact way to show how the energy of harmonics shifts across the bands over time. Figure 3a shows that over February the RMS amplitude generally decreases across higher harmonic bands, and the later dates (toward February 28) tend to have larger amplitudes extending further into higher bands compared to earlier dates, indicating a shift of harmonic energy toward higher orders with time. Whereas in Figures 3b–3c there are a gradual increase in harmonic energy and persistence of stronger amplitudes into higher bands toward the end of February. Therefore, from the RMS analysis of the A_p index we can conclude that while 2001 highlights a relative weakening of amplitudes with increasing harmonic bands but a shift of energy toward higher orders by late February, 2003 and 2017 demonstrate a more systematic buildup of harmonic energy across bands, with stronger and more persistent amplitudes sustained into higher bands as the month progresses, indicating enhanced geomagnetic variability toward the end of February. In 2001, all bands are very smooth functions of time. They drop on February 11 and partially recover after February 19. The drop is smoother for 0–19 and sharper for the higher order bands. In 2003, there was a drop on February 15 and a recovery after February 18. It was in reverse to the general trend. A similar pattern was observed in 2017. There was a drop on February 14 and a recovery after February 16. The band 40–59 grew on February 14 and dropped after February 16, while 100–109 did not recover from the drop.

Contour plots of modified and normalized phase ϕ_{nl} are demonstrated in Figure 4. Eqs. (8)–(10) yield values between 0° and 360° . We modified ϕ_{nl} to make it continuous (by adding or subtracting a multiple of 360°). Consequently ϕ_{nl} was normalized through division by n. The contour plots show that modified and normalized ϕ_{nl} nearly monotonically decreases with time. And Figure 5 demonstrates that this decrease is nearly linear. Figure 6 displays RMS of modified and normalized ϕ_{nl} . During the solar maximum (2001, 2003), the band 1–19 hits 90° in the beginning, while during relatively quiet period (2017), it hits 0° in the beginning. The other bands of the phase angles show similar temporal profiles, hitting nearly 0° in the beginning.

The right part of Eq. (2) suggest a complex form of A_p ,

$$A_p^c(t) = \sum_{n=0}^{N} c_{nl} e^{i\left\{n\omega\left[t - \left(\frac{l}{K} + \frac{1}{2}\right)T\right] - \phi_{nl}\right\}}.$$
(14)

The real part of A_p^c is equal to A_p . Hodographs (Figure 7) show us behavior of the complex A_p^c . A hodograph represents the path traced out by the tip of a vector (here a complex number) as it moves over time. No physical conclusions are drawn from the imaginary part. The hodographs reveal clear differences in geomagnetic activity across solar cycle phases: February 2001 (solar maximum) shows large, widely spread loops indicating intense storm activity, while February 2003 exhibits more compact trajectories with moderate disturbances. By contrast, February 2017 (solar minimum) shows fewer and tighter loops, reflecting quieter geomagnetic conditions.





4 Conclusions

Fourier analysis of the linearly interpolated A_p index is performed. The coefficients near $\cos n\omega t$ and $\sin n\omega t$ are found The Fourier reconstruction of A_p works well. One can add an imaginary counterpart and thus hodographs can be plotted. The hodograph of February 2017 is uniformly spread over the complex surface, while those of 2001 and 2003 reveal a tendency for concentrations in a region close to the origin. This could be general properties of quiet and disturbed periods. From contour plots for phase angles and amplitudes, we noticed that phase angles can serve as precursors in estimations of possible future increases of the A_p index level. The Fourier coefficient magnitudes and phases change smoothly with time, while the index A_p is not very smooth. This opens a way for extrapolation of the magnitudes and phases and a possible use of them for determination of A_p in future times.

Author contributions. E.R. suggested the method for harmonic analysis of A_p index, M.V. derived the formulas, performed calculations of the coefficients, and made all figures. T.I. developed Python codes. T.H. studied literature and developed codes. P.M. performed calculations. S.K. made a formal analysis. All authors wrote the text and made editing.

185 Competing interests. No competing interests are present.

Acknowledgements. This research was supported by the NSF grant 2230363. M. V. acknowledges support from the AV ČR grant RVO:67985815.





References

195

- Abe, O. E., Fakomiti, M. O., Igboama, W. N., Akinola, O. O., Ogunmodimu, O., and Migoya-Orue, Y. O.: Statistical analysis of the occurrence rate of geomagnetic storms during solar cycles 20–24, Advances in Space Research, 71, 2240–2251, 2023.
- Ahluwalia, H. S.: A_p time variations and interplanetary magnetic field intensity, Journal of Geophysical Research: Space Physics, 105, 27 481–27 487, 2000.
 - Campbell, W. H.: Spectral composition of geomagnetic field variations in the period range of 5 min to 2 hr as observed at the earth's surface, Radio Science, 8, 929–932, 1973.
 - Cliver, E. W., Boriakoff, V., and Bounar, K. H.: The 22-year cycle of geomagnetic and solar wind activity, Journal of Geophysical Research: Space Physics, 101, 27 091–27 109, 1996.
 - Cooley, J. W., Lewis, P. A., and Welch, P. D.: The fast Fourier transform and its applications, IEEE Transactions on Education, 12, 27–34, 1969.
 - de Gonzalez, A. L., Gonzalez, W. D., Dutra, S. L., and Tsurutani, B. T.: Periodic variation in the geomagnetic activity: A study based on the A_p index, Journal of Geophysical Research: Space Physics, 98, 9215–9231, 1993.
- 200 De Michelis, P., Consolini, G., and Tozzi, R.: On the multi-scale nature of large geomagnetic storms: an empirical mode decomposition analysis, Nonlin. Processes Geophys., 19, 667–673, 2014.
 - Delouis, H. and Mayaud, P. N.: Spectral analysis of the geomagnetic activity index *aa* over a 103-year interval, Journal of Geophysical Research, 80, 4681–4688, 1975.
- Idosa, C., Giri, A., Mosisa, E., and Gashu, C.: Variations of cosmic ray intensity with the solar flare index, coronal index, and geomagnetic indices: Wavelet and cross correlation approaches, Physics of Plasmas, 30, 083 901, 2023.
 - Le Mouel, J. L., Lopes, F., and Courtillot, V.: Singular spectral analysis of the aa and D_{st} geomagnetic indices, Journal of Geophysical Research: Space Physics, 124, 6403–6417, 2019.
 - Love, J. J.: Secular trends in storm-level geomagnetic activity, Annales Geophysicae, 29, 251–262, 2011.
- Pai, G. L. and Sarabhai, V. A.: Periodic fluctuations in the geomagnetic field during magnetic storms, Planetary and Space Science, 12, 855–865, 1964.
 - Rangarajan, G. K. and Lyemori, T.: Time variations of geomagnetic activity indices K_p and A_p : an update, Annales Geophysicae, 15, 1271–1290, 1997.
 - Riabova, S.: Application of wavelet analysis to the analysis of geomagnetic field variations, Journal of Physics: Conference Series, 1141, 012 146, 2018.
- 215 Riabova, S. A. and Spivak, A. A.: Variations in the K-index of geomagnetic activity in the Moscow Region, Izvestiya, Atmospheric and Oceanic Physics, 54, 705–710, 2018.
 - Rigozo, N. R., Echer, E., and Vieira, L. E. A.: Spectral analysis of sunspot number and geomagnetic indices (1868–2001), Journal of Atmospheric and Solar-Terrestrial Physics, 68, 182–190, 2006.
- Shnirman, M. G., Le Mouël, J. L., and Blanter, E. M.: The 27-day and 22-year cycles in solar and geomagnetic activity, Solar Physics, 258, 220 167–179, 2009.
 - Zajtsev, A. N., Ivanov, K. G., and Odintsov, V. I.: Structure and nature of spectra of the geomagnetic field in the case of very large magnetic storms (13–14 March 1989 and 8–9 Nov. 1991), Geomagnetism and Aeronomy, 33, 145–150, 1993.





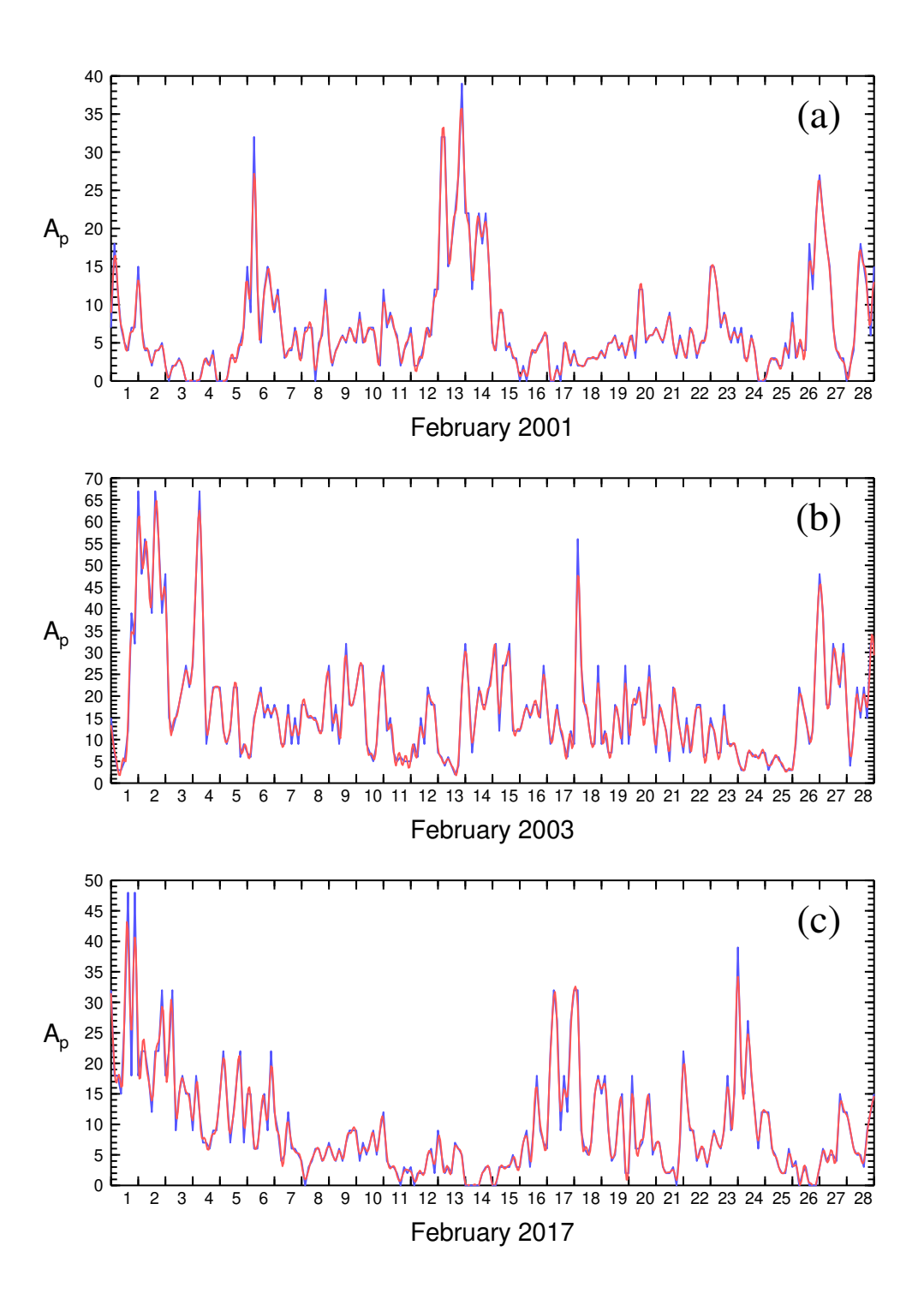


Figure 1. A_p time profiles for our three time periods. The blue lines represent the original data, and the red lines the reconstructed A_p .





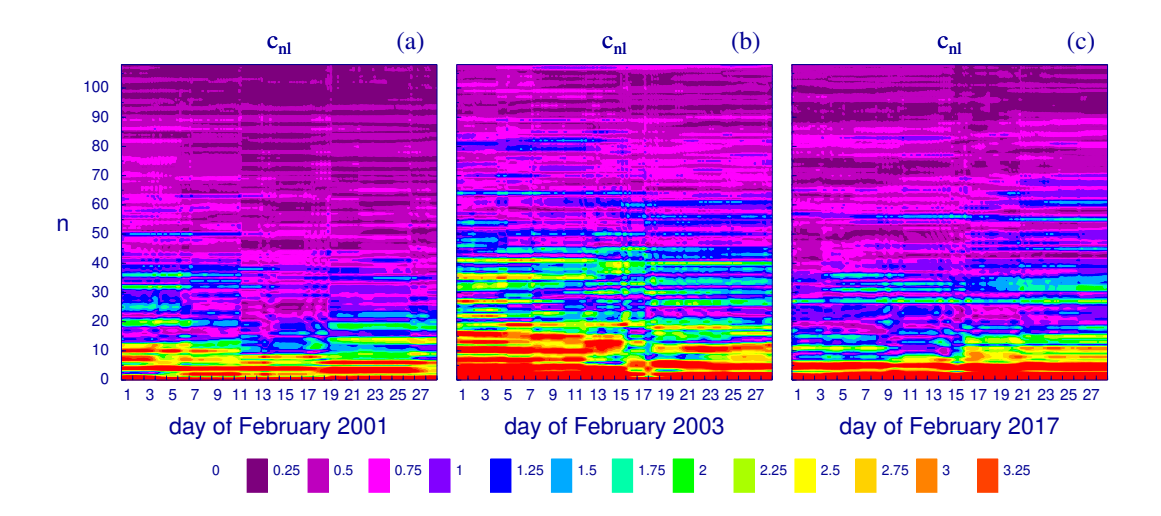


Figure 2. Contour plots of c_{nl} for our three period under consideration.





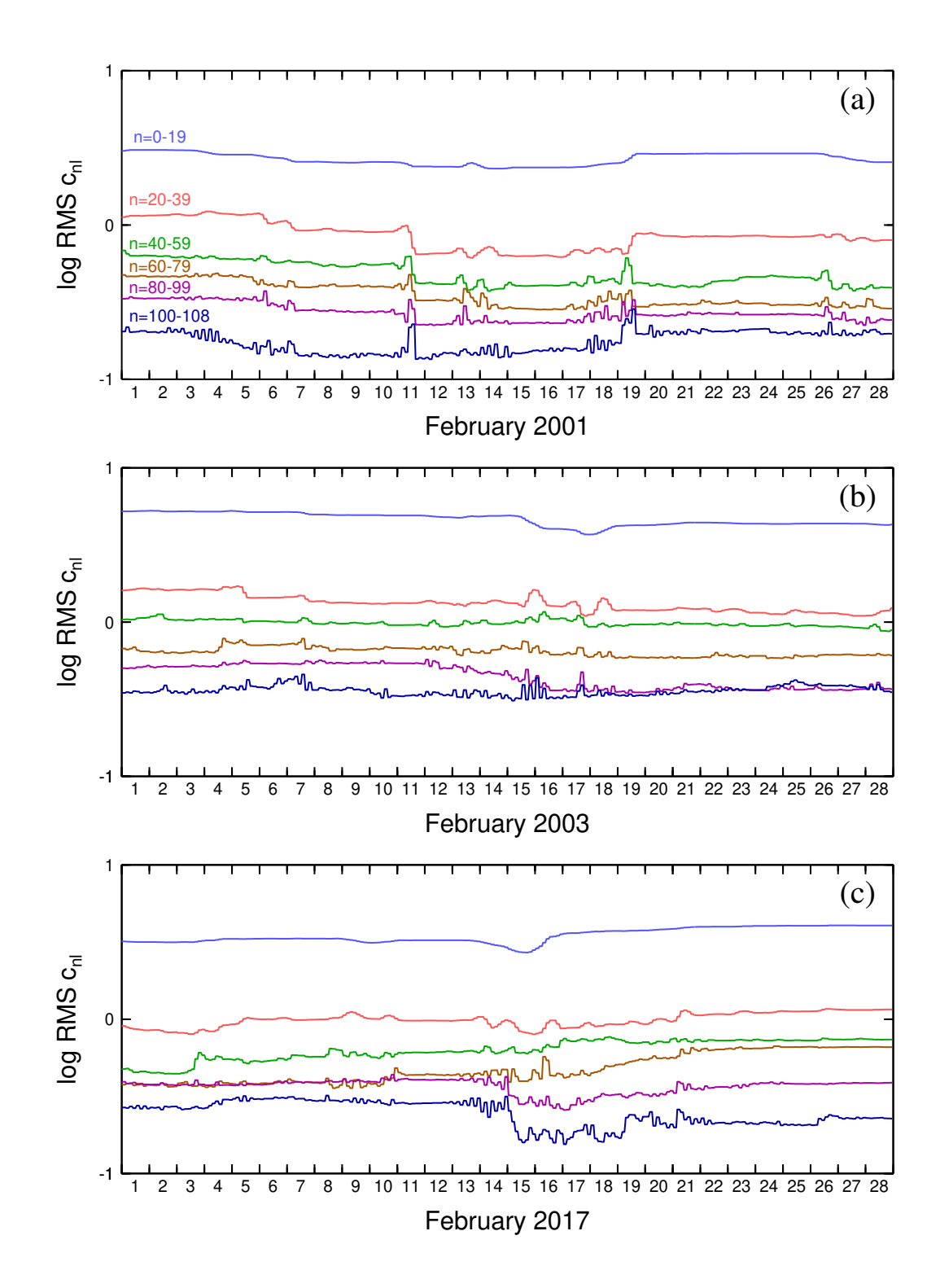


Figure 3. Profiles of RMS of c_{nl} for six bands of n, distinguished by colors. Color-coding of parts (b) and (c) is the same as of (a).





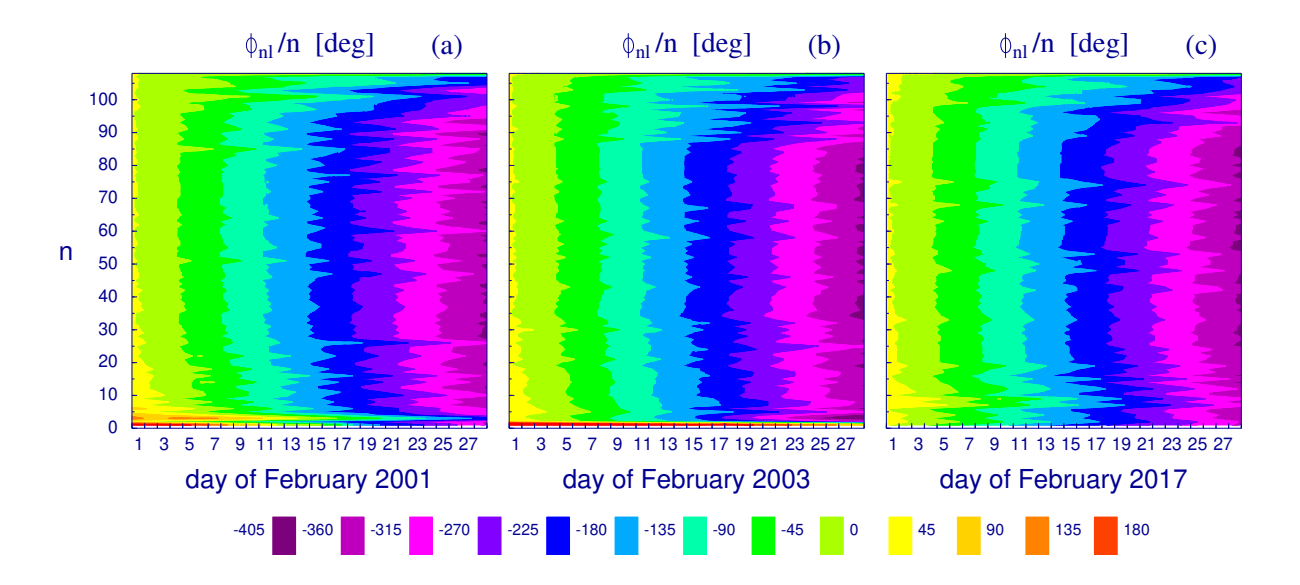


Figure 4. Contour plots of modified and normalized ϕ_{nl} .

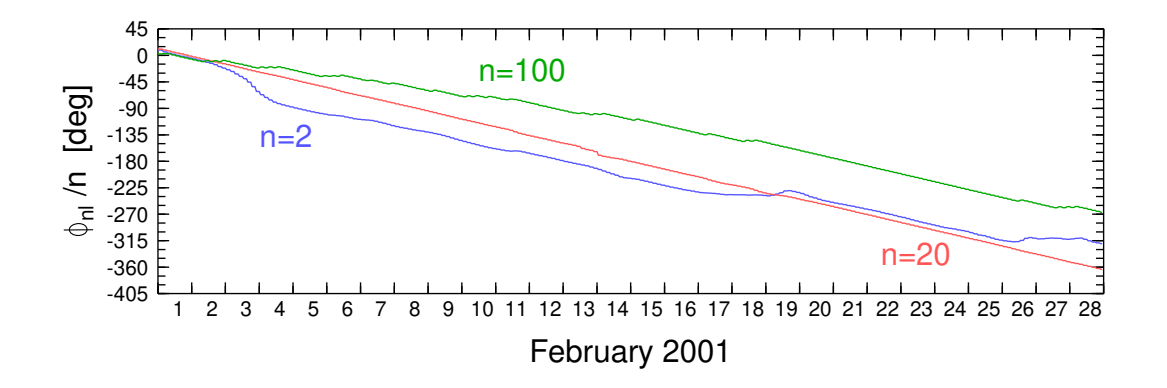


Figure 5. Profiles of modified and normalized ϕ_{nl} for three n in February 2001.





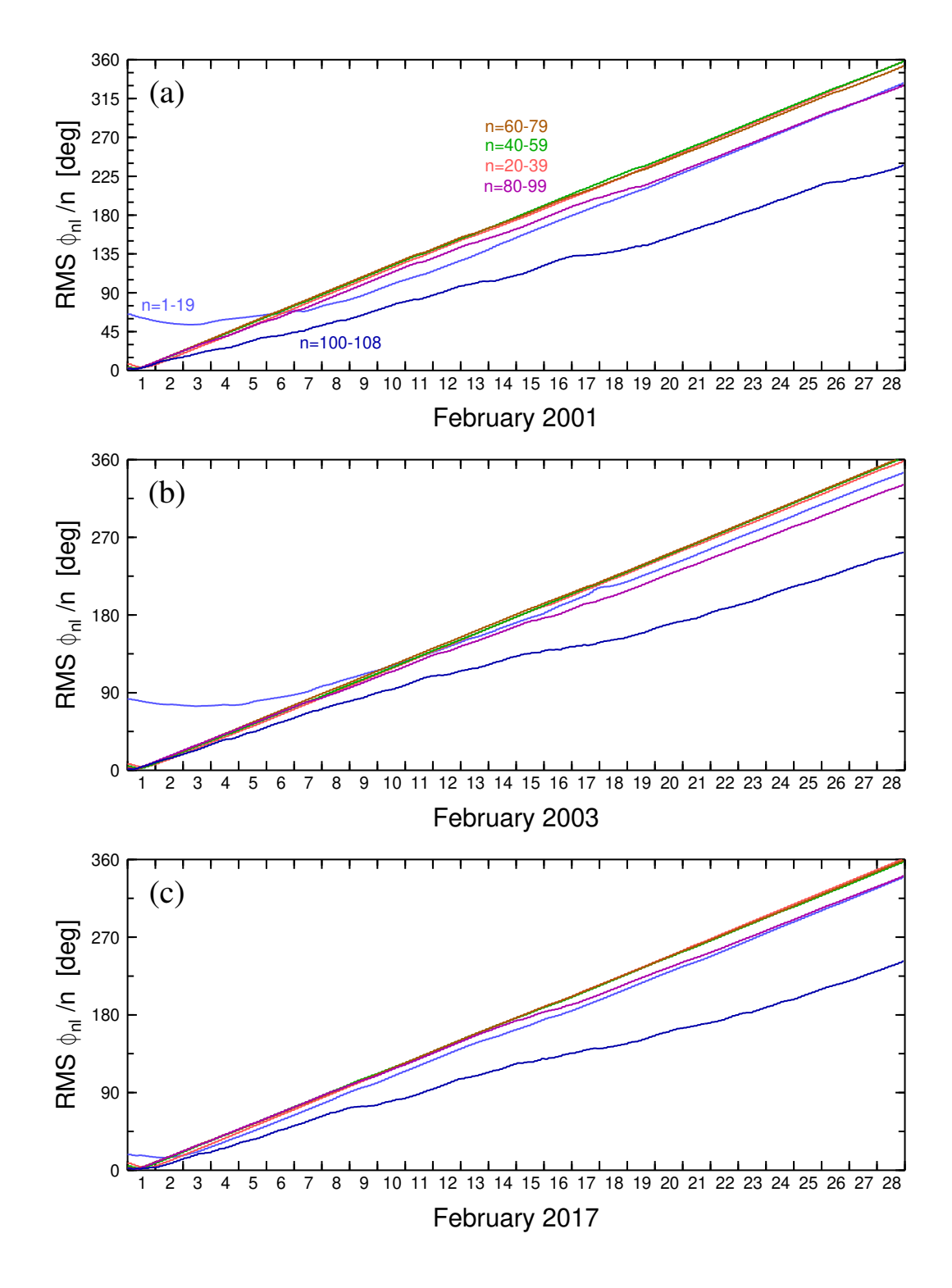


Figure 6. Profiles of RMS of modified and normalized ϕ_{nl} for six bands of n, distinguished by colors. Color-coding of parts (b) and (c) is the same as of (a).





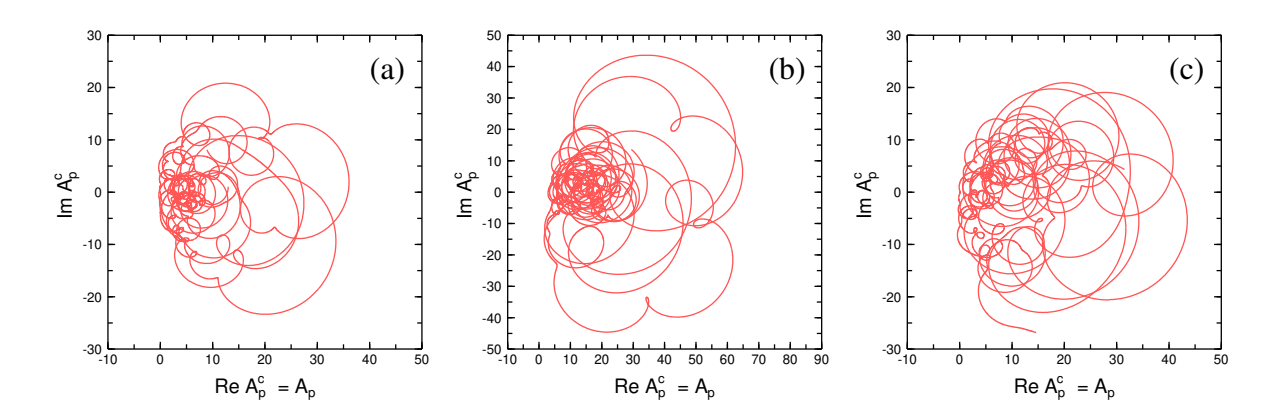


Figure 7. Hodographs of the complex A_p^c .